Boundary-Layer Meteorol (2012) 145:165–184
DOI 10.1007/s10546-011-9650-0

ARTICLE

An Alternative Eddy-Viscosity Model for the Horizontally Uniform Atmospheric Boundary Layer

J. D. Wilson

Received: 13 January 2011 / Accepted: 26 July 2011 / Published online: 24 August 2011

Abstract This paper explores the utility of specifying the eddy viscosity for the horizontally uniform boundary layer as the product $K = \sigma_w^2 \tau_w$ of the variance of vertical velocity and an empirical time scale τ_w, as opposed to the more usual formulation $K = \sqrt{\alpha k}\lambda_k$ where k is the turbulent kinetic energy (TKE), λ_k is a length scale and α is a dimensionless coefficient. Simulations were compared with the observations on Day 33 of the Wangara experiment, and with a plausible specification of τ_w (or λ_k) each model simulated convective boundary-layer development reasonably well, although the $K = \sqrt{\alpha k}\lambda_k$ closure produced a more realistic width for the entrainment layer. Under the light winds of Day 33, and with the onset of evening cooling, an excessively shallow and strongly-stratified nocturnal inversion developed, and limited its own further deepening. Boundary-layer models that neglect radiative heat transport and parametrize convective transport by eddy viscosity closure are prone to this runaway (unstable) feedback when forced by a negative (i.e. downward) surface flux of sensible heat.

Keywords Atmospheric boundary layer · Boundary-layer modelling · Eddy-viscosity closure · First-order closure · Nocturnal boundary layer

1 Introduction

As early as the 1970s it was anticipated that higher-order closure would soon provide a better basis for the practical modelling of the atmospheric boundary layer (ABL) than had eddy-viscosity closure, which for a long time had been understood to be wrong in principle. Nevertheless the eddy-viscosity approach remains very much in evidence to this day, and not only in the present generation of numerical weather forecast models (e.g. the Canadian Meteorological Centre's "Global Environmental Multiscale" model, GEM) where it serves in the parametrization of subgrid transport in the ABL, but also in numerical studies

J. D. Wilson (✉)
Department of Earth and Atmospheric Sciences, University of Alberta, Edmonton, AB T6G 2E3, Canada
e-mail: jaydee.uu@ualberta.ca

(e.g. of the Martian boundary layer: Savijärvi and Kauhanen 2008; Davy et al. 2009) that focus on the meteorology per se (as opposed to fundamentals of closure). The durability of eddy-viscosity/diffusivity closure despite its known naïvety surely has much to do with the quest for computational speed and robustness (i.e. reliably obtaining the flux–gradient relationship approximately correctly, and rarely getting it excessively wrong), whereas the higher-order closure approach continues to attack special cases, and in its latest guise offers a daunting number of tuning constants (e.g. Cheng et al. 2005). Furthermore in practise the performance of higher-order closure models for the ABL has not been regarded as superior to that of the simpler models in terms of overall practicality and fidelity (e.g. Manins 1982; Hess and Garratt 2002).

Readers will probably be familiar with the variety of eddy-viscosity (K) closures, and the dominance of those in which the square root of the turbulent kinetic energy (TKE, k) is assigned the role of a velocity scale in the prescription $K = \sqrt{\alpha k}\lambda_k$ of the eddy viscosity (λ_k being the accompanying length scale, and α a closure constant). Departing from that pattern, and with a view to improving the treatment of "wall-blocking" at the base of the *inner* region of the wall shear layer, Durbin (1991) suggested instead equating the velocity scale to the standard deviation of the velocity component normal to the wall, so that $K = \sigma_w^2 \tau_w$ where τ_w is a turbulence time scale[1] (Pope 2000, Sec. 11.7.2). Although Durbin invoked considerations of tensor invariance as confirming this choice, a more intuitive justification lies in Taylor's (1921) Lagrangian theory of dispersion, and Batchelor's (1949) reconciliation of it with the eddy diffusion paradigm (e.g. Wyngaard 2010, Sec. 4.3.2). Furthermore a suggestive insight that emerges from connecting the needed closure for K with Taylor's theory is that both the velocity scale and the associated length scale are (or should be) properties of the vertical motion field,[2] which perhaps explains the paradox that while most eddy viscosity parametrizations tune the ABL length scale to the local gradient Richardson number, which responds to the mean wind shear as well as the thermal stratification, some authors (e.g. Galperin et al. 1988) have reported ABL simulations using a non-local closure (Bougeault and Lacarrère 1989) that sensitizes the outer-layer length scale to the profile of mean potential temperature alone.[3] Then is the Richardson number (R_i, defined below as Eq. 47) a primary influence on K in the outer layer? The proper velocity and time scales for the eddy viscosity being statistics of the vertical motion, perhaps not—given that the variance σ_w^2 is driven by *buoyant* production, and sensitive to wind shear (and shear production of TKE) only via the redistribution term. And if (hypothetically) it is a false turn to consider R_i a primary factor influencing K in the outer layer, that false turn entrains the conundrum that in general there is no definitive or simple *pattern* to the velocity shear in the outer layer, so that tuning K to R_i may entail a misguided and fruitless search for pattern.

Setting aside those speculations and turning to fact, with only a few exceptions (e.g. Karcz and Badur 2005) Durbin's plausible suggestion for modelling the eddy viscosity is scarcely reflected in the vast body of work using K closures. The purpose of this paper, then, is to suggest that the $K = \sigma_w \lambda_w (\equiv \sigma_w^2 \tau_w)$ closure for the ABL ought to perform no less well than the more familiar choices based on $\sqrt{k}$ as a velocity scale, and conceivably (although this is a speculation, and certainly not proven here) might perform better. The motivation

[1] This is the pattern used in second-order closure models (e.g. Rao et al. 1974; Launder et al. 1975), which model the vertical transport of Reynolds stresses (and other needed quantities) using an effective diffusivity $\sigma_w^2 \tau_w$.

[2] It is implicit here that the eddy viscosity is applied to model *vertical* fluxes in a horizontally-uniform ABL. As Durbin (1993) notes, this eddy viscosity would be "inappropriate to complex geometries."

[3] Such calculations have also been performed by the author but those results will not be shown here; they are not categorically outside the span of the results that are shown.

and perspective here differ from Durbin's, in that the focus is the *outer* layer of the ABL, for the eddy viscosity in the surface layer is given by Monin–Obukhov similarity theory (MOST). However there is no inconsistency relative to Durbin's reasoning, and probably the main distinction is that here the TKE dissipation rate ϵ is prescribed by the simplistic but robustly popular formulation $\epsilon \propto k/\tau_k$ rather than by solving the conventional "black box" epsilon equation. The utility of the latter is subject to scepticism (e.g. Cheng et al. 2002), and from their survey of K models for the stratified ABL Weng and Taylor (2003) concluded that "models with TKE and a diagnostic equation for (length scale) are quite good, while closures with TKE and a prognostic equation for (length scale) do not guarantee success although these models do carry more physical processes."

2 Overview of Eddy-Viscosity Models for the ABL

Numerous authors (e.g. Holt and Raman 1988; Alapaty et al. 1997; Hess and Garratt 2002; Weng and Taylor 2003) have reviewed eddy-viscosity treatments of the ABL. "K-profile" schemes (e.g. Troen and Mahrt 1986; Noh et al. 2003) specify a profile of K directly, but entail the difficulty that ABL depth (δ) must be prescribed. The Prandtl class of schemes uses an algebraic specification of the length scale λ and diagnoses the velocity scale (say, "q") from the cross-stream mean velocity shear, symbolically $q = \lambda \partial_z U$. Another class of schemes associated (Launder and Spalding 1972) with Prandtl and Kolmorogov also specifies λ algebraically, but sets $q = \sqrt{k}$ (Bradshaw et al. (1967) are often credited with originating the numerical implementation of this idea; Delage (1974) is a meteorological example that will feature later), and there are many variants of the two-equation scheme where both q and λ are in effect computed interactively with the main flow properties (meteorological applications of the $k - \epsilon$ scheme to the ABL include Detering and Etling 1985; Duynkerke and Driedonks 1987; Apsley and Castro 1997). As to the relative merits of these schemes, Holt and Raman (1988) concluded "TKE closure is preferable to first-order closure in predicting the overall turbulence structure of the boundary layer," while Apsley and Castro (1997) "make no claim that solving a conservation-type equation for the length-scale-determining variable (ϵ) is necessarily better than an algebraic specification of the length scale *for flow over homogeneous terrain*" (italicized by Apsley and Castro).

Making sense of the vast literature on eddy-viscosity modelling of the ABL—or more specifically, attempting to learn what is the most suitable eddy-viscosity closure for a given purpose—is complicated by these several factors:

1. Differing specifications for closure constants and/or uncertain meteorological parameters map each of the above four primary schemes into a multitude of particular calculations, some of whose inter-variability could doubtless be categorized as owing to the "noise" originating in these arbitrary choices. Without attempting to be all-inclusive as to sources of flexibility in the models, one easily observes varied choices for constants (and even functional forms) appearing in the "universal" Monin–Obukhov functions, which not infrequently, for application in the outer layer, are adjusted away from consensus values appropriate to the surface layer; for the ratios of eddy diffusivities to the eddy viscosity (turbulent Prandtl number and Schmidt number); and for the limiting length scale λ_∞ for the ABL, often attributed to Blackadar (1962).
2. Although it is known that grid-independent solutions for the ABL demand high vertical resolution (Delage 1997), many authors have studied solutions that were known *not* to be grid-independent—the context having been application of the closure within numerical weather forecast models, wherein the luxury of high resolution is unavailable.

3. The focus of authors has ranged widely, e.g. identification of a workable scheme for ABL parametrization in numerical weather prediction (Benoit et al. 1989; Bélair et al. 1999); numerical issues, e.g. computational instability of Prandtl-type (and other) K-closures (Davies 1983; Girard and Delage 1990; Deleersnijder et al. 2003); analysis/interpretation of terrestrial boundary-layer experiments; and exploratory simulations of Martian micrometeorology (e.g. Savijärvi and Kauhanen 2008; Davy et al. 2009).

One might form the impression that the field of enquiry has been saturated with effort, and that further research on the eddy viscosity for one-dimensional ABL models would be futile. One very justifiably might assume that one or several or even all of the existing treatments is/are good enough, and that any further objective refinement (as opposed to tinkering with coefficients to procure better agreement with some particular case) is unlikely to be possible. Alternatively, and without entertaining the delusion that there exists an "ultimately correct" eddy-viscosity model, perhaps one may usefully ask whether there is a more *rational* model, or simply a less arbitrary (better behaved or constrained) model. That present day treatments of the ABL could bear improvement is implicit in the fact that it may be necessary to place bounds on ABL depth to circumvent unrealistic calculations; e.g. GEM's daytime ABL depth is limited to $\delta \leq \delta_{\mathrm{mx}}$, and instances where the limiting value prevails are common (R. d'Amours, pers. comm., 2011).

The following sections will demonstrate a straightforward application of $K = \sigma_w^2 \tau_w (\equiv \sigma_w \lambda_w)$ closure to the uniform ABL. Solutions, which will be compared with the observations of Wangara Day 33, are to all practical purposes grid- (and timestep-)independent, and resolve the surface layer.

3 The Numerical Model

Under eddy diffusion closure the horizontal momentum equations in the horizontally-uniform ABL simplify to

$$\frac{\partial U}{\partial t} = \frac{\partial}{\partial z}\left[K\frac{\partial U}{\partial z}\right] + f\left(V - V_{\mathrm{g}}\right), \tag{1}$$

$$\frac{\partial V}{\partial t} = \frac{\partial}{\partial z}\left[K\frac{\partial V}{\partial z}\right] - f\left(U - U_{\mathrm{g}}\right), \tag{2}$$

where $U_{\mathrm{g}}, V_{\mathrm{g}}$ parametrize the synoptic scale horizontal pressure gradient. Similarly the conservation equations for potential temperature and for specific humidity are

$$\frac{\partial \theta}{\partial t} = \frac{\partial}{\partial z}\left[P_r^{-1} K\frac{\partial \theta}{\partial z}\right], \tag{3}$$

$$\frac{\partial Q}{\partial t} = \frac{\partial}{\partial z}\left[S_c^{-1} K\frac{\partial Q}{\partial z}\right], \tag{4}$$

where P_r, S_c are the turbulent Prandtl and Schmidt numbers, here assumed here to be unity[4] (the distinction between the eddy viscosity and eddy diffusivities will be sustained by

[4] This is in the spirit of a rough approximation; why should these ratios not only be independent of position and of particulars of the flow and of the distribution of sources and sinks of heat and water vapour, but even contrive to be unity?

retaining these symbolic factors). The parametrized TKE and variance (σ_w^2) equations are

$$\frac{\partial k}{\partial t} = K\left[\left(\frac{\partial U}{\partial z}\right)^2 + \left(\frac{\partial V}{\partial z}\right)^2\right] - \frac{g}{\theta_0 P_r} K \frac{\partial \theta}{\partial z} - \epsilon + \frac{\partial}{\partial z}\left[\frac{1}{\gamma} K \frac{\partial k}{\partial z}\right], \tag{5}$$

$$\frac{\partial \sigma_w^2}{\partial t} = -2\frac{g}{\theta_0 P_r} K \frac{\partial \theta}{\partial z} - \epsilon_{ww} + R_{ww} + \frac{\partial}{\partial z}\left[\frac{1}{\gamma} K \frac{\partial \sigma_w^2}{\partial z}\right], \tag{6}$$

where the terms on the right-hand sides respectively represent shear and/or buoyant production, dissipation (ϵ or ϵ_{ww}), redistribution (R_{ww}), and turbulent plus pressure transport (θ_0 is the mean Kelvin temperature; simulations used $\gamma = 1$). The eddy viscosity/diffusivity and the dissipation rates were modelled algebraically as

$$K = \sigma_w^2 \tau_w (\equiv \sigma_w \lambda_w), \tag{7}$$

$$\epsilon_{ww} = c_2 \frac{\sigma_w^2}{\tau_w}, \tag{8}$$

$$\epsilon = \frac{3}{2}\epsilon_{ww}, \tag{9}$$

where τ_w is the needed empirical time scale and c_2 is a constant. The redistribution term in Eq. 6 was modelled as

$$R_{ww} = c_1 \frac{\Sigma_w^2 - \sigma_w^2}{\tau_w}, \tag{10}$$

(Rotta's model; Pope 2000, Sec. 11) where Σ_w^2 represents the level of σ_w^2 for which redistribution would vanish, specified as $\Sigma_w^2 = 2k/3$. As computational speed was of no interest here, both the k- and the σ_w^2-equations were solved. A speedier alternative would be to solve for σ_w^2 alone, adopting a plausible profile for the ratio k/σ_w^2 (as noted by a reviewer, however, this would mean that the influence of mean wind shear on σ_w^2 via its influence on k, however important or unimportant that should be, would be neglected). With these specifications the model equation for σ_w^2 may be written

$$\frac{\partial \sigma_w^2}{\partial t} = -2\frac{g}{\theta_0 P_r}\sigma_w^2 \tau_w \frac{\partial \theta}{\partial z} - c_2 \frac{\sigma_w^2}{\tau_w} + c_1 \frac{2k/3 - \sigma_w^2}{\tau_w} + \frac{\partial}{\partial z}\left[\gamma^{-1}\sigma_w^2 \tau_w \frac{\partial \sigma_w^2}{\partial z}\right]. \tag{11}$$

More elaborate treatments were examined, but results did not differ qualitatively from those shown below.

3.1 Requirement that the Model Reproduce a Reference Flow

It is useful to think in terms of a *calibration* of the above equations, such that they should exactly reproduce analytically (and, to within the level of error caused by discretization, numerically) the structure of the horizontally-homogeneous and neutrally-stratified atmospheric surface layer (hh_NSL). Regarding this reference flow, it is legitimate to assume steady state, to neglect the Coriolis terms as well as vertical gradients of mean

fluxes, and to assume the TKE and σ_w^2 budgets are in local equilibrium. Then with the specifications

$$\tau_w = \frac{k_v u_* z}{\sigma_w^2}, \tag{12}$$

$$\sigma_{u,v,w} = c_{u,v,w} u_*, \tag{13}$$

$$k = \alpha^{-1} u_*^2, \tag{14}$$

$$\alpha = \frac{2}{c_u^2 + c_v^2 + c_w^2}, \tag{15}$$

$$c_1 = \frac{2c_w^{-2}}{c_u^2 + c_v^2 + c_w^2}, \tag{16}$$

$$c_2 = \frac{2}{3} c_w^{-4} \tag{17}$$

(where k_v is the von Karman constant, here assumed to be 0.4, and u_* is the friction velocity), Eqs. 1–9 reduce to a set of simultaneous algebraic equations whose solution reproduces the idealized paradigm of the constant-stress layer (inner region of a wall shear layer), viz.

$$U = \frac{u_*}{k_v} \ln \frac{z}{z_0}, \tag{18}$$

$$\epsilon = \frac{u_*^3}{k_v z}, \tag{19}$$

$$\overline{u'w'} = -K \frac{\partial U}{\partial z} = -u_*^2, \tag{20}$$

$$K = k_v u_* z \equiv \sigma_w^2 \tau_w. \tag{21}$$

(Note: depending on whether one considers the eddy viscosity of the ideal hh_NSL as being formed with u_* or with σ_w the corresponding length scale is $k_v z$ or $k_v u_* z/\sigma_w$). The value prescribed for α corresponds to one's choice of the values of normalized velocity standard deviations $\sigma_u/u_* = c_u$, etc in the reference flow. Here (except where noted in Sect. 4.5) $\alpha = 1/4.84$, corresponding to $\sigma_u/u_* = \sigma_v/u_* = 2$, $\sigma_w/u_* = 1.3$.

It may occur to readers that the model coefficients could have been calibrated relative to a *stratified* reference state, for example invoking local equilibrium (in the spirit of an approximation) and obtaining $\alpha = \alpha(z/L)$ etc., where L is the Obukhov length. There are logical difficulties with that approach: whether L be chosen as the surface value or as a local scale, it is not apparent why Monin–Obukhov scaling should apply outside the surface layer. In any case no promising progress was made by pursuing this idea.

3.2 Formulation for the ABL Time Scale

Holt and Raman (1988) tabulated many previous authors' formulations for the needed length scale in $K = \sqrt{\alpha k} \lambda_k$ schemes, and it is useful to emphasize the critical role of this choice: having surveyed many K closures Weng and Taylor (2003) stated that "differences in model results with different turbulence closures are primarily caused by the way the turbulent length scales are modelled."

Following common practice[5] here the time scale has been parametrized by inverse summation,

$$\frac{1}{\tau_w} = \frac{1}{\tau_{w,SL}} + c_{\mathrm{BV}} N + \frac{1}{\tau_\infty}. \tag{22}$$

The first term on the right-hand side is (the reciprocal of) the surface-layer time scale, and its value is given by MOST. According to MOST the mean wind shear and the eddy viscosity in the surface layer are

$$\frac{\partial U}{\partial z} \equiv \frac{u_*}{k_{\mathrm{v}} z} \phi_m \left(\frac{z}{L} \right), \tag{23}$$

$$K = u_* \frac{k_{\mathrm{v}} z}{\phi_m \, (z/L)} = \sigma_w^2(z) \tau_w(z), \tag{24}$$

where L is the Obukhov length[6]

$$L = \frac{-\theta_0 u_*^3}{k_v g \overline{w'\theta'}} \tag{25}$$

and $\phi_m(z/L)$ is a universal dimensionless function. Hence

$$\tau_{w,SL} = \frac{k_{\mathrm{v}} u_* z}{\sigma_w^2 \phi_m(z/L)}. \tag{26}$$

The present calculations use

$$\phi_m = (1 - 28z/L)^{-1/4}, \quad L < 0, \tag{27}$$

$$= (1 + 5z/L), \quad L \geq 0, \tag{28}$$

(cf. Dyer and Bradley 1982). The second term in Eq. 22 invokes a buoyancy frequency

$$N = 0, \quad \partial\theta/\partial z \leq 0 \tag{29a}$$

$$N = N_{\mathrm{BV}} \equiv \left(\frac{g}{\theta_0} \frac{\partial \theta}{\partial z} \right)^{1/2}, \quad \partial\theta/\partial z > 0, \tag{29b}$$

i.e. the time scale of any stably-stratified sublayer of the ABL is (potentially) determined by the Brunt–Vaisala frequency N_{BV} (cf. Galperin et al. 1988). Finally the time scale τ_∞ serves to limit the integral scale in a neutral or unstable outer layer (cf. the λ_∞ invoked as maximum length scale in the $\sqrt{\alpha k}\lambda_k$ closure, a value that may be assigned an auspicious constant value, or prescribed by one of Blackadar's (1962) relations relating λ_∞ alternatively to G/f or to u_*/f, where G is the geostrophic wind speed).

It is interesting to note that in the stable case the rate of buoyant production of TKE may be written

$$\frac{g}{\theta_0} \overline{w'\theta'} = -\frac{g}{\theta_0} \sigma_w^2 \tau_w P_r^{-1} \frac{\partial \theta}{\partial z} = -\sigma_w^2 \tau_w P_r^{-1} N_{\mathrm{BV}}^2. \tag{30}$$

The same term (multiplied by 2) appears in the σ_w^2 equation, and results in a σ_w^2 destruction term that is linearly proportional to σ_w^2.

[5] Gryning et al. (2007) briefly survey the origins of common heuristic formulae for the ABL length scale. The inverse summation approach ensures asymptotically correct behaviour of the length scale in two or more layers.

[6] Except in Sect. 4.5, L is based on surface fluxes and is height independent.

3.3 Numerical Method

3.3.1 Grid

Variance/TKE (σ_w^2, k) gridpoints were staggered relative to U gridpoints, at which not only U but also V, θ, Q were stored. The lowest TKE node lay at the roughness height $z = z_0$, the lowest U node at z_P (above z_0), and the highest U node at the upper boundary $z = Z_{\rm mx}$. U nodes (at heights labelled z_u) were centrally placed between their neighbouring k nodes (z_k).

The grid was built by stepping upward from $z_k(1) \equiv z_0$ in steps Δz_k that were uniform below a specified height z_1 and, above that level, were stretched by a factor of 1.2 in each successive layer until attaining a limiting maximum value $\Delta z_{k,\rm mx}$. The grid can be reproduced from the specified values of z_0 and ($\Delta z_{k,\rm min}$, z_1, $\Delta z_{k,\rm mx}$, $Z_{\rm mx}$) and for simulations shown here the values used were (0.05, 1, 10, 2000), resulting in 244 grid levels.

3.3.2 Discretization

Prior to discretization the governing equations were integrated analytically across the "control layer" surrounding the node. Taking the U-momentum equation for example, and supposing the Jth control layer spans $z_1 \le z \le z_2 \equiv z_1 + \Delta z_u$, a Crank–Nicolson method was used, viz.

$$\begin{aligned}\Delta z_u(J)\frac{U_J^{n+1}-U_J^n}{\Delta t} &= \frac{1}{2}\left[K\frac{\partial U^{n+1}}{\partial z}\right]_{z_1}^{z_2}+\frac{1}{2}\left[K\frac{\partial U^{n}}{\partial z}\right]_{z_1}^{z_2}\\ &+\frac{f}{2}\left[V_J^{n+1}-V_g^{n+1}\right]\\ &+\frac{f}{2}\left[V_J^{n}-V_g^{n}\right]\end{aligned} \tag{31}$$

where the profile of geostrophic wind speed is provided (known). The momentum fluxes across the control-layer faces were specified according to the pattern

$$\left(K\frac{\partial U}{\partial z}\right)_{z_1} = K(z_1)\frac{U_J - U_{J-1}}{\Delta z_k(J)}, \tag{32}$$

such that the solution at the "new" time level $n+1$ was obtained as

$$\mathbf{M}\,\mathbf{U}^{n+1} = \mathbf{B}, \tag{33}$$

where the coefficient matrix $\mathbf{M}$ is tridiagonal, and $\mathbf{B}$ depends only on the known solution at the earlier time n. In practice, due to the coupling of the equations with each other and with the evolving profile of eddy viscosity, a solution update $n \to n+1$ (i.e. timestep) progressed by iteration through trial solutions (symbolically ${}^m\mathbf{U}^{n+1}$) and the matrices $\mathbf{M}$, $\mathbf{B}$ also evolved from iteration to iteration along with the evolving eddy viscosity, etc. To facilitate convergence, relaxation was applied when iterating through trial solutions and as a precaution physical eddy viscosities/diffusivities were augmented by an artificial diffusivity $K^*(= 10^{-5}\mathrm{m}^2\,\mathrm{s}^{-1})$. For simulations reported here the timestep $\Delta t = 5$ s, but results differed negligibly with $\delta t = 45$ s.

3.3.3 Boundary Conditions and the Treatment of Surface Drag

As the lowest gridpoint for (U, V, θ, Q) at "z_P" lay above ground, the lower face of the corresponding control layer was at ground level, and the surface fluxes were supplied. The heat and vapour fluxes were prescribed by the measurements and the usual wall-layer method was used to infer a surface friction velocity u_* from the velocities U_P, V_P at z_P using the measured value of the roughness length, viz.

$$u_*^2 = C_D \left(U_P^2 + V_P^2\right) \tag{34}$$

where

$$C_D = \left[\frac{k_v}{\ln(z_P/z_0)}\right]^2. \tag{35}$$

The lowest gridpoints for k, σ_w^2 lay on the ground, and boundary values were supplied as

$$k = [\phi_{uu} + \phi_{vv} + \phi_{ww}]\, u_*^2/2, \tag{36}$$

$$\sigma_w^2 = \phi_{ww} u_*^2, \tag{37}$$

where ϕ_{uu}, etc are the universal MO functions for the velocity variances.

In the case that $z_1 \equiv z_0$, surface drag in the x-direction features within Eq. 31 through a term having the form $(-K\,\partial U/\partial z)_{z_1}$. This was parametrized as

$$-\left(K\frac{\partial U}{\partial z}\right)_{z_0} = -C_D U_P \sqrt{U_P^2 + V_P^2} \tag{38}$$

and split into the two contributions, i.e. those at time levels $(n, n+1)$. A treatment (of source terms) given by Patankar (1980) ensured that the drag would oppose the flow, whatever the orientation of the latest iterative guess ${}^m U_P^{n+1}$. Analogous steps were taken for drag in the y-direction.

At the upper boundary, placed high enough to exceed the ultimate depth of the ABL, (U, V, θ, Q) were assigned their measured "free stream" values, while vertical gradients in k, σ_w^2 were zeroed.

4 Simulations: Wangara Day 33

The Wangara boundary-layer experiment (Clarke et al. 1971; Hess et al. 1981) was performed in July and August 1967 at Hay, New South Wales (34°30′S, 144°56′E). Innumerable investigators (e.g. Deardorff 1974; Wyngaard and Coté 1974; André et al. 1978; Yamada and Mellor 1975; Chen and Cotton 1983; Alapaty et al. 1997) have tested numerical models of the ABL against the observations of Wangara Day 33, this particular day being chosen due to its simplicity—there being (Deardorff 1974) "clear skies, very little horizontal advection of heat or moisture, and lack of any frontal activity within 1000 km." The season being (late) southern hemisphere winter, radiative forcing was of modest strength, and the available energy $Q^* - Q_G$ (net radiation less the soil heat flux density) peaked at a little over 200 W m^{-2} around noon local time (EST). Winds were relatively light, such that the Blackadar length scale

$$\lambda_\infty = 0.00027\frac{G}{f} \tag{39}$$

was only about 10 m.

4.1 Forcing—Boundary Conditions and Pressure Gradient

In view of the decision to resolve the surface layer, the approach taken was to use the measured time series of the available energy $Q^* - Q_G$ and to partition this assuming a fixed value for the Bowen ratio (for Day 33 it was assumed that $Q_{H0}/Q_{E0} = 10$). In contrast, many authors have "driven" simulations of Day 33 by using measured near-ground properties: for example Yamada and Mellor (1975) imposed the observed screen height time series of virtual temperature as their lower boundary condition on that property. Drag at the ground (i.e. momentum flux) was computed using the wall-layer approach documented earlier, with $z_0 = 0.0037$ m (as used by previous authors). At the upper boundary the time-dependent measured values of (U, V, θ, Q) were imposed, with linear interpolation between measurement times.

Following Deardorff the "x-component (eastward pointing) of the geostrophic wind…was taken to vary linearly from $-5.5\,\mathrm{m\,s^{-1}}$ at the surface to $-2.6\,\mathrm{m\,s^{-1}}$ at 1 km to $-1.2\,\mathrm{m\,s^{-1}}$ at 2 km," i.e. U_G was taken as height-dependent, but constant in time. Conversely, and departing from Deardorff by whom it was taken as zero at all heights and times, V_g was here treated as height-independent but varying in time with linear interpolation on the 3-h interval. Deardorff had noted that (with his choices) "both components are in rough agreement with the Wangara data for this day," and his choice for the profile of the geostrophic wind has been adopted by several subsequent authors (e.g. Wyngaard and Coté 1974; Chen and Cotton 1983). On the other hand Hess et al. (1981) deprecated the accuracy of the Wangara estimates for the thermal wind.

4.2 Initialization

Following the precedent of other authors whose focus has been the daytime, fairweather boundary layer, here the simulation was initialized from the profiles at 0900 EST. More specifically, piecewise-linear initial profiles of U, V, θ, Q were constructed, and the conservation equations solved in steady state mode with these profiles fixed, to extract consistent initial profiles of σ_w^2, k. The starting profiles are shown on the diagrams to follow; it is noteworthy that the initial profile of potential temperature reveals a residual adiabatic (mixed) layer sandwiched between the ground-based nocturnal inversion and a capping inversion aloft (e.g. Fig. 2).

4.3 Results: $K = \sigma_w^2 \tau_w$ Closure

Figure 1 indicates that the $K = \sigma_w^2 \tau_w$ closure yields qualitatively reasonable daytime evolution of the scalar profiles θ, Q even when implemented with a naïve specification of the empirical time scale, viz. an unamended extrapolation to all heights of the surface-layer formulation implied by MOST,

$$\tau_w = \frac{k_v u_* z}{\phi_m(z/L)\sigma_w^2} \tag{40}$$

(the Obukhov length L being based on the surface fluxes). A more critical inspection reveals that at 1200 EST the modelled mixed layer (whether judged by the θ or the Q profiles) is too shallow whereas at 1500 EST it is too deep,[7] and that in general the entrainment layer is

[7] Although the surface sensible heat input has been prescribed by the measurements, the entrainment heat flux is computed subject to the inaccuracy that stems (a) from the use of eddy-diffusion closure in this type of flow (large eddies; possible counter-gradient transport); and (b) from the parametrization of K, which is unlikely to be accurate in the entrainment layer.

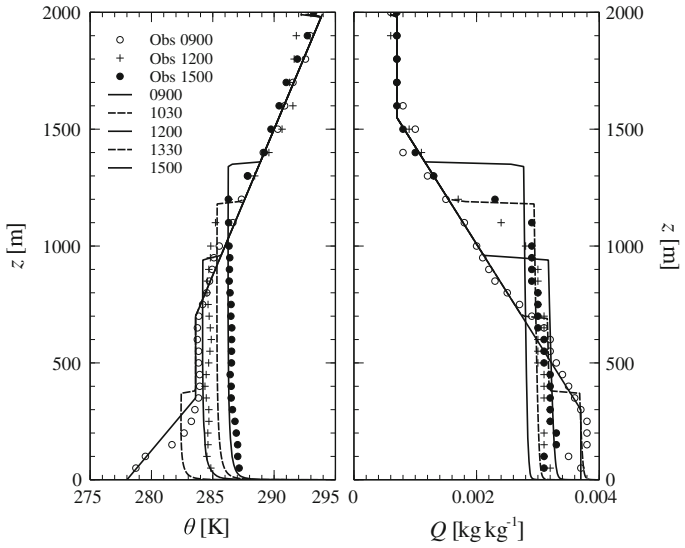

Fig. 1 Numerical simulation of Wangara Day 33, using the $K = \sigma_2^2 \tau_w$ closure with $\tau_w = k_v u_* z / (\sigma_w^2 \phi_m(z/L))$, i.e. the MOST-based surface-layer formulation applied without amendment at all heights (L being the Obukhov length based on surface fluxes)

too thin (i.e. abrupt and shallow). Given that the mixed layer and the entrainment layer are defined and identified in contradistinction to each other, perhaps these flaws of the computed scalar profiles share the same cause; e.g. a thicker entrainment layer at 1500 EST might (ipso facto) improve the depth of the mixed layer. The fact of the entrainment zone being too thin presumably signifies inadequate mixing in that region, where strongly stable stratification suppresses σ_w^2, and one cannot attribute that lack of mixing to a too small τ_w, for Eq. 40 surely *overestimates* its value far aloft. If σ_w^2 is being too severely attenuated at the top of the mixed layer, potential adjustments to the computational scheme might include imposition of a minimum value (for σ_w^2, perhaps as a function of the surface heat flux); increasing the transport term by reducing the dimensionless factor γ (in Eqs. 5, 11); or adopting more complex formulations for redistribution and/or dissipation. No such tuning is attempted here.

Had the initial temperature profile (on Wangara Day 33) not featured a capping inversion, Eq. 40 in conjunction with the $\sigma_w^2 \tau_w$ closure would have permitted sensible heat injected at the surface to be mixed through a deeper layer. If the scheme is to be capable of general application the time scale τ_w cannot be permitted to increase ad infinitum with increasing height. Figure 2 was computed using

$$\frac{1}{\tau_w} = \frac{\phi_m}{k_v z} \frac{\sigma_w^2}{u_*} + c_{BV} N + \frac{1}{\tau_\infty} \tag{41}$$

with $\tau_\infty = 10$ min and $c_{BV} = 1$ (the Brunt–Vaisala frequency in the capping inversion was $N_{BV} \approx 0.17$ Hz; the fitted surface inversion at 0900 EST has $N_{BV} = 0.24$ Hz). Outcomes (not shown) differing almost negligibly from Fig. 2 were obtained with ($c_{BV} = 0$, $\tau_\infty = 10$–15 min) and with ($c_{BV} = 1$, $\tau_\infty = \infty$), i.e. it is redundant (in this case) to have included two terms in Eq. 41 limiting the growth of τ_w with height (however, had the initial θ profile been neutral, the term in N would have been ineffective). This (more justifiable) parametrization for τ_w has modestly improved the simulation of the scalar profiles, and if the 1200 EST mixed layer remains too shallow it must be noted that the same deficiency features with $\sqrt{\alpha k} \lambda_k$

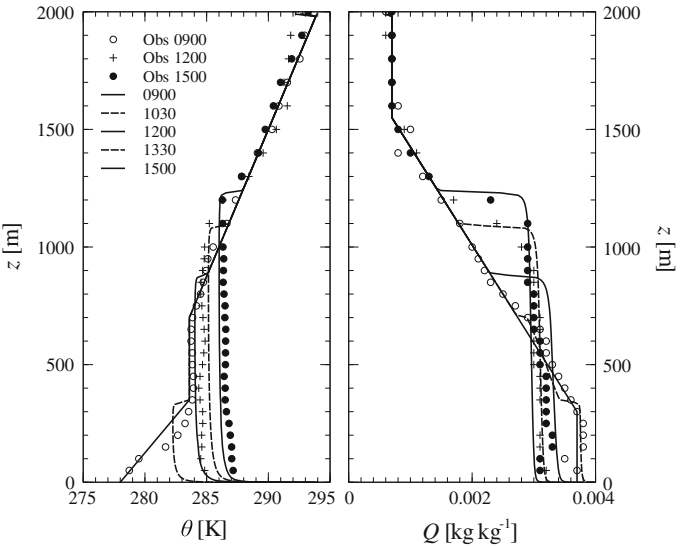

Fig. 2 Day 33, using the $K = \sigma_w^2 \tau_w$ closure with $1/\tau_w = \sigma_w^2 \phi_m/(k_v u_* z) + c_{BV} N_{BV} + 1/\tau_\infty$ ($c_{BV} = 1$, $\tau_\infty = 10$ min). *Note* although its exact value is unknown, certainly the surface humidity flux was small, so that the daytime evolution in $Q(z)$ essentially reflects re-mixing throughout a deepening mixed layer

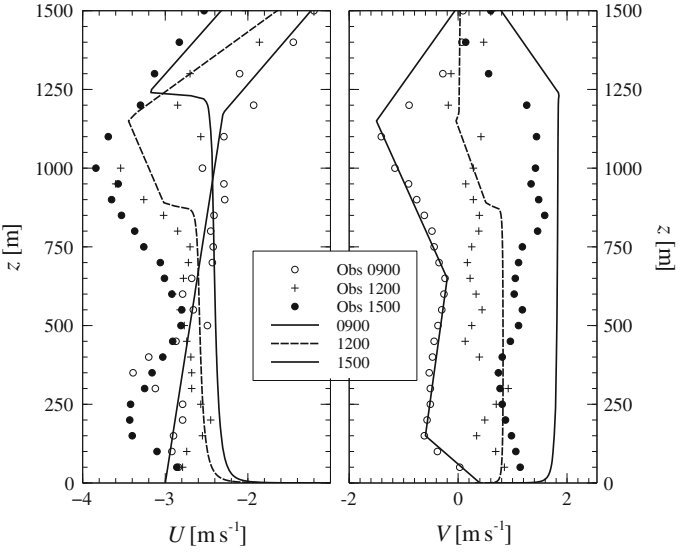

Fig. 3 Modelled wind profiles corresponding to simulation of Figure 2 for Wangara Day 33, in comparison with observed winds from the Wangara pilot balloon network

closure (see Fig. 6). Outside the entrainment layer the computed daytime θ profiles from the $K = \sigma_w^2 \tau_w$ closure scheme are in satisfactory agreement with the soundings (potential temperature discrepancies do not exceed about 1–2 K), particularly since the latter cannot be expected to have properly resolved the surface layer (note the stronger lapse rate of the model near the ground than is reflected by the lowest pair of observations).

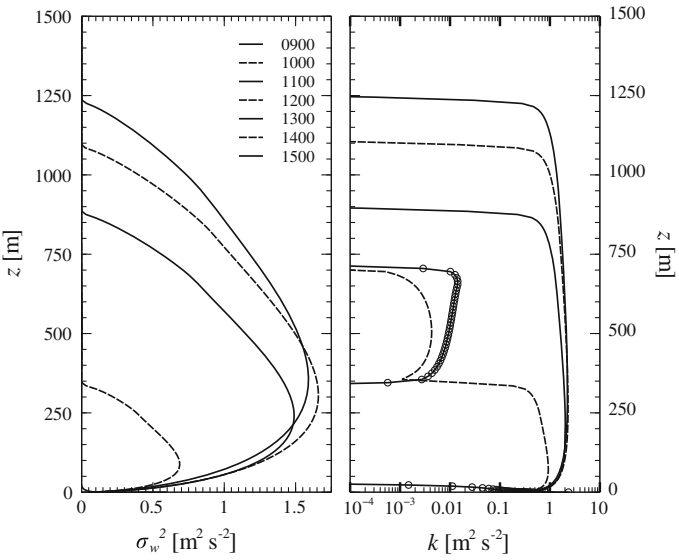

Fig. 4 Modelled profiles of the vertical velocity variance and TKE corresponding to simulation of Fig. 2. *Open circles* designate the profile of k at initialization, featuring a turbulent surface layer and a residual mixed layer aloft

Not surprisingly, however, the simplistic K closure is less skillful in its prediction of the wind profiles (Fig. 3), which were by no means uniform in the "mixed layer." Unlike the $(\theta,\ Q)$ profiles, model wind profiles are extremely sensitive to prescription of the mean pressure gradient ∇P (equivalently, the profiles of the geostrophic velocity components), i.e. the essential forcing. In view of the several possibilities afforded by the Wangara observations, alternative prescriptions of $U_G(z)$, $V_G(z)$ were tried before settling on that given in Sect. 4.1. Irrespective of the choice of turbulence closure, one finds that the quality of computed wind profiles hinges on how realistically (or otherwise) $\nabla P(z)$ is prescribed and whether the assumption of horizontal homogeneity was legitimate.

Turning now to the computed profiles of vertical velocity variance and TKE, Fig. 4 shows that their overall form is plausible (the Wangara experiment did not provide observations). Focusing on the profile of σ_w^2 at 1500 EST when the ABL depth was $\delta \approx 1250$ m, the maximum variance (about $1.6\,\mathrm{m^2\,s^{-2}}$) occurs at $z \approx 350$ m, i.e. at a normalized height $z/\delta \approx 0.3$. This is consistent with the pattern from aircraft observations (in the convective boundary layer) as summarized by

$$\frac{\sigma_w^2}{w_*^2} = 1.8\left(\frac{z}{\delta}\right)^{2/3}\left(1 - 0.8\frac{z}{\delta}\right)^2, \tag{42}$$

(Hunt et al. 1988, Eq. 2.13a; Kaimal and Finnigan 1994, Eq. 1.51), which equation gives maximum variance at $z/\delta = 0.31$. As to the magnitude of the peak, again focusing on 1500 EST[8] the convective velocity scale evaluates to

$$w_* \equiv \left(\frac{g}{\theta_0}\delta\frac{Q_{H0}}{\rho c_p}\right)^{1/3} \approx 1.7\,\mathrm{m\,s^{-1}} \tag{43}$$

[8] $\theta_0 \approx 287$ K, $Q_{H0} \approx (10/11) \times 164\,\mathrm{W\,m^{-2}}$, $\rho_0 \approx 1.25\,\mathrm{kg\,m^{-3}}$.

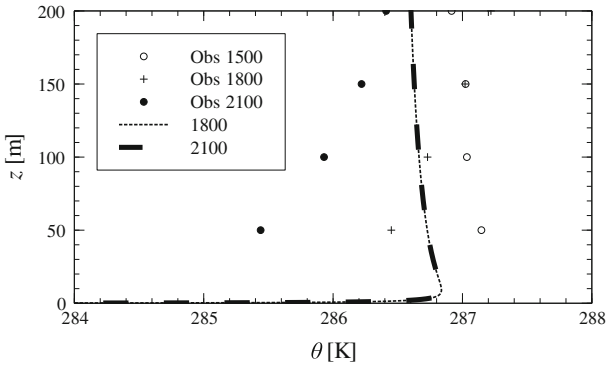

Fig. 5 Evening cooling on Day 33, simulated using the $K = \sigma_w^2 \tau_w$ closure with $1/\tau_w = \sigma_w^2 \phi_m/(k_V u_* z) + c_{BV} N + 1/\tau_\infty$ ($c_{BV} = 1$, $\tau_\infty = 10$ min)

so that the model profile of σ_w^2/w_*^2 peaks with a maximum value of about 0.6, this too being in acceptable agreement with aircraft observations (e.g. Hunt et al. 1988, Fig. 7a).

4.3.1 Simulation of the Cooling Phase

Figure 5, a continuation of the simulation giving the daytime phase shown by Fig. 2, reveals a persistent flaw of simulations of nocturnal cooling during light winds: evening heat loss is restricted to an excessively shallow layer, resulting in an excessively strong inversion. This peculiarity results not only when using the $K = \sigma_w^2 \tau_w$ closure, but also with every variant of $K = \sqrt{\alpha k} \lambda_k$ closure here examined.[9]

How is this to be interpreted? One can intuit (from the conservation equations for k, σ_w^2) that there is a positive feedback in operation in any inversion layer (stable stratification suppresses k, σ_w^2 in turn limiting the depth of the layer participating in cooling), but these simulations fly in the face of observation. One is left with two possible explanations: either this behaviour is inherent in the equations solved, or, it is a (false) consequence of the discretization and numerical procedure. Regarding the latter possibility, many variations of the scheme have been tested, closely following the recommendations of Patankar (1980), without any significantly different outcome (Patankar 1981, notes "source-term linearization is often a very crucial operation; it is responsible for computational success in many complex situations"). This peculiar outcome for nocturnal cooling in light winds appears to be inherent to the model equations. Truly drastic and unacceptable interventions were needed to prevent it, namely, removal of the buoyant production terms in the k, σ_w^2 equations and setting $\beta_s = 0$ in the MOST function $\phi_m = 1 + \beta_s(z/L)$ for stable stratification (cf. Eq. 28). More complex model equations for σ_w^2 were investigated, for example adding the "isotropization of production" contribution to the redistribution term in the σ_w^2 budget. The character of the nocturnal inversions was unaltered. We return to this idiosyncracy of the eddy-viscosity model(s) below.

[9] A reviewer stated "this kind of problem has been observed for quite some time at operational Numerical Weather Prediction centres" and "often occurs for weak winds, clear-sky conditions with strong radiative cooling and weak turbulent exchange."

4.4 Results: $K = \sqrt{\alpha k}\lambda_k$ Closure

It was suggested earlier that the $K = \sigma_w^2 \tau_w$ closure should be no *less* useful than the (almost universally preferred) $K = \sqrt{\alpha k}\lambda_k$ closure, and the results of the previous section are now compared with a calculation that typifies results from the latter. The TKE was computed (as before) from Eq. 5, and the length scale, following one of the prescriptions of Bélair et al. (1999), as

$$\frac{1}{\lambda_k} = \phi_m(z)\left[\frac{1}{k_v z} + \frac{1}{\lambda_\infty}\right], \tag{44}$$

with $\lambda_\infty = 200$ m and

$$\phi_m = (1 - 40R_i)^{-1/6}, \quad R_i < 0, \tag{45}$$

$$= (1 + 12R_i), \quad R_i > 0, \tag{46}$$

where R_i is the gradient Richardson number

$$R_i = \left(\frac{g}{\theta_0}\right) \frac{\partial\theta/\partial z}{(\partial U/\partial z)^2 + (\partial V/\partial z)^2}. \tag{47}$$

Figure 6 was computed with a limiting value $R_i \leq 0.5$ imposed in Eq. 46, a step that increased the penetration of the mixed layer into the capping inversion. As with the $\sigma_w^2 \tau_w$ closure, the depth of the mixed layer at 1200 EST is underestimated and when the simulation of Fig. 6 is continued into the evening cooling phase an unrealistically sharp and shallow nocturnal inversion occurs—again, just as with the $\sigma_w^2 \tau_w$ closure. The simulated wind profiles from this scheme (not shown) were qualitatively similar to (and no better or worse than) those of the $\sigma_w^2 \tau_w$ scheme, i.e. they were highly sensitive to the geostrophic wind components and did not exhibit the undulations with height ("unmixed" profiles) seen in the observations.

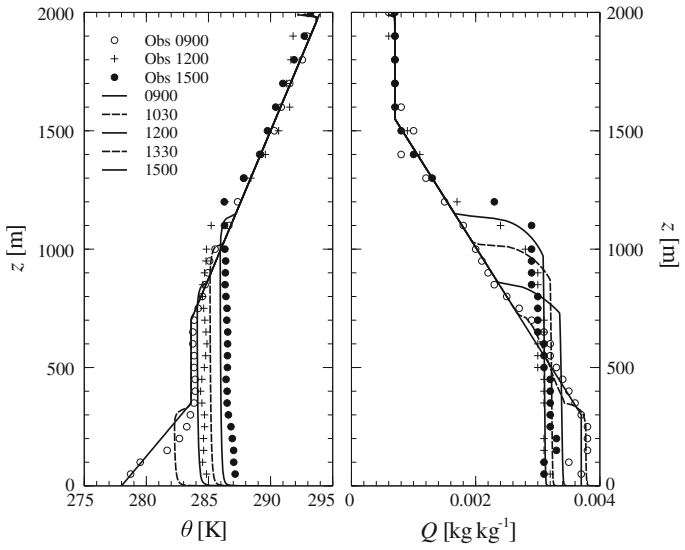

Fig. 6 Day 33 simulated using the Bélair et al. (1999) $K = \sqrt{\alpha k}\lambda_k$ closure, with a limit ($R_i \leq 0.5$) imposed in the calculation of $\phi_m(R_i)$

It is however noticeable that the humidity profile of Fig. 6 features a broader entrainment layer than produced by the $\sigma_w^2\tau_w$ closure (Fig. 2). This may reflect the fact that, within the capping inversion layer, the TKE is sustained by shear production, counterbalancing (to some extent) the buoyant suppression that dominates the σ_w^2 budget.[10] If so, this implies a better formulation is needed for the redistribution and dissipation terms in the σ_w^2 equation, if the $\sigma_w^2\tau_w$ closure is to better simulate the entrainment zone.

4.5 Evening Cooling Phase: Comparison with Delage's Variant of the $K = \sqrt{\alpha k}\lambda_k$ Closure

In this section we divert temporarily from our main objective, viz. to establish the potential usefulness of $K = \sigma_w^2\tau_w$ closure, in order to determine whether the (unexpected) outcome of the present simulations of nocturnal cooling is or is not consistent with earlier work. Delage (1974) reported simulations of the development of the nocturnal boundary layer from an initially neutral state, driven by an imposed rate of cooling of the surface temperature and with the length scale prescribed as

$$\frac{1}{\lambda_k} = \frac{1}{k_v(z+z_0)} + \frac{\beta_s}{k_v L(z)} + \frac{1}{\lambda_\infty} \tag{48}$$

where $\beta_s = 5$, $\lambda_\infty = 0.0004G/f$ (cf. Eq. 39), and $L(z)$ is a *local* Obukhov length. Delage stated his "model is characterized by the use of local quantities in the determination of the eddy exchange coefficient. Radiative heat transfer is neglected for simplicity—to restrict the number of external parameters—on the basis that it plays a minor part in the formation of the inversion in moderate and strong winds, except close to the ground." Accordingly many of Delage's results, presented in dimensionless form, correspond to rather a strong geostrophic wind such that the Rossby number

$$R_o \equiv \frac{G}{z_0 f} = 10^7. \tag{49}$$

Figure 7, which corresponds to (and agrees closely with) Delage's Figure 3, was computed using a domain depth $Z_{\rm mx} = 1000$ m, roughness length $z_0 = 0.01$ m, Coriolis parameter $f = 10^{-4}\,{\rm s}^{-1}$ and geostrophic wind speed $G = 10\,{\rm m\,s}^{-1}$. These choices exactly replicate Delage's $R_o = 10^7$ and the rate of surface cooling exactly matches that given by his Eqs. 10, 11 (with $D = 200$). As in Delage's calculation, the depth of the inversion does not ascend above $fz/G \approx 15 \times 10^{-4}$ or $z \approx 150$ m. The friction velocity, which is not imposed, stabilized at $0.31\,{\rm m\,s}^{-1}$ across all the profiles shown—and this sufficed to sustain mixing and stave off the outcomes reported above for evening cooling of Wangara Day 33, a day with much lighter winds aloft.

Here for application to Wangara Day 33 the Delage closure was initialized with a uniform potential temperature of 287 K (corresponding roughly to the observation at 1800 h), and driven by an imposed surface heat flux. Irrespective of the magnitude of the latter, if the geostrophic wind was reduced below about $9\,{\rm m\,s}^{-1}$ numerical instability resulted—whereas there is no indication Delage's implementation exhibited this phenomenon. Figure 8 shows that when $G = 10\,{\rm m\,s}^{-1}$ and $(\overline{w'\theta'})_0 = -0.02\,{\rm K\,m\,s}^{-1}$ the inversion grows to a depth of order $z = 100$ m, but that the stronger cooling rate actually observed at 1800 on Day 33 results in a much shallower inversion. This is consistent with Delage's remark that (depending on the Rossby number) "the final depth of the inversion (h) increases by 45–80% when the cooling rate is reduced by a factor 2." The trend of these simulations, viz. atmospheric

[10] However simulations reported by Witek et al. (2011) using $K = \sqrt{\alpha k}\lambda_k$ closure also show a very shallow entrainment zone.

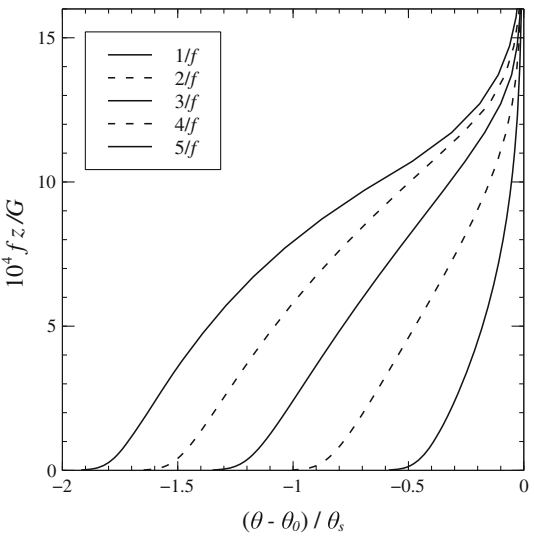

Fig. 7 Nocturnal cooling from an initially neutral state, computed using Delage's variant of the $K = \sqrt{\alpha k}\lambda_k$ scheme with $R_o = 10^7$, $D = 200$, $f = 10^{-4}$, $G = 10\,\mathrm{m\,s^{-1}}$, $z_0 = 0.01\,\mathrm{m}$, and using Delage's value (0.16) for the equilibrium coefficient u_*^2/k (his "c"). Driven by Delage's prescribed rate of cooling of the surface, and plotted at time intervals $1/f$. (For this case, equivalent to that of Delage's Figure 3, the Delage scaling temperature is $\theta_s = 6.116\,\mathrm{K}$)

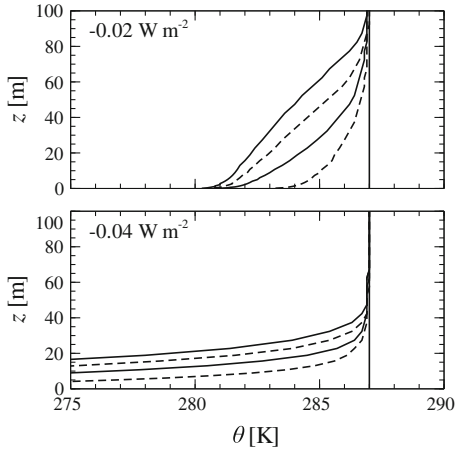

Fig. 8 Nocturnal cooling, starting from an initially neutral state, with geostrophic wind speed $G = 10\,\mathrm{m\,s^{-1}}$. Prescribed surface kinematic heat flux: *upper panel* $-0.02\,\mathrm{K\,m\,s^{-1}}$, *lower panel* $-0.04\,\mathrm{K\,m\,s^{-1}}$. Computed using Delage's variant of the $K = \sqrt{\alpha k}\lambda_k$ scheme

heat loss being confined to an increasingly shallower layer as G decreases and/or surface cooling increases, is broadly consistent with the findings of earlier sections.

5 Conclusion

To the extent that σ_w and $\sqrt{k}$ are roughly proportional, the suggestion of using the former instead of the latter as the needed velocity scale in forming the eddy viscosity may appear trivial. However it seems worthwhile to reserve judgement, in case making the distinction should offer a greater payoff than expected. As noted earlier, in general a $K = \sigma_w^2 \tau_w$ closure should result in a reduced sensitivity of the outer-layer eddy viscosity to the shear of the horizontal wind components, an element that is far from being a universal aspect of the ABL and not well simulated even by higher-order closures.

Daytime simulations with the $K = \sigma_w^2 \tau_w$ closure have proven comparable to those with the $K = \sqrt{\alpha k} \lambda_k$ closure, albeit with an underestimated width for the entrainment zone that suggests the need for a refinement of the σ_w^2 equation. One might remark that reasonable agreement with the daytime observations has been procured (only) by virtue of tuning (of the formulation for τ_w), but this is no more the case in reference to the $\sigma_w^2 \tau_w$ closure than in reference to the alternatives (notably the many published variants of $K = \sqrt{\alpha k} \lambda_k$ closure). The author does not claim of Eq. 22 that it is the optimal parametrization for τ_w (nor of Eq. 44 that it is the optimal formulation for λ_k). Only by comparing the model(s) with many observed cases might one hope to extract such a recommendation, but a survey of the literature suggests that decades of work using $K = \sqrt{\alpha k} \lambda_k$ closure have not culminated in an unambiguously best prescription for λ_k. Thus for the time being interest in $K = \sigma_w^2 \tau_w$ closure more appropriately centres on its *rationality* than on any question of its practical superiority.

The physically unrealistic outcomes computed for evening cooling, viz. an excessively strong but shallow nocturnal inversion, raised an interesting question: did this happen merely as an artifice of numerical procedure, or was it a genuine implication of the mathematical models investigated? Prolonged investigation suggests this behaviour is intrinsic to the equations. The mechanism is not mysterious. Stable stratification certainly does suppress to *some* extent the fluctuating vertical motion, and the notion that boundary-layer turbulence can be sustained only if the Richardson number remains below some critical (albeit not very well defined) value is surely sound. Radiative divergence, long since known to be important during evenings with light winds (e.g. Schaller 1977; André et al. 1978; Garratt and Brost 1981; André and Mahrt 1982; Ha and Mahrt 2003; Siqueira and Katul 2010), is without doubt the *essential* physical and (in models of this type) mathematical element that, during light winds and strong surface cooling, enables sensible heat to be drawn from a layer of macroscopic depth (say, order some 100 m), rather than from the almost infinitesimal chilled layer produced by convection-only treatments.

Acknowledgments This work has been supported by the Natural Sciences and Engineering Research Council of Canada. Helpful feedback was provided by two unknown reviewers. Graphs were created using the free software "Veusz."

References

Alapaty K, Pleim J, Raman S, Niyogi D, Byun D (1997) Simulation of atmospheric boundary layer processes using local- and nonlocal-closure schemes. J Appl Meteorol 36:214–233

André J, Mahrt L (1982) The nocturnal surface inversion and influence of clear-air radiative cooling. J Atmos Sci 39:864–878

André J, Moor G, Lacarrere P, Therry G, Vachat R (1978) Modeling the 24-hour evolution of the mean and turbulent structures of the planetary boundary layer. J Atmos Sci 35:1861–1883

Apsley D, Castro I (1997) A limited-length-scale $k-\epsilon$ model for the neutral and stably-stratified atmospheric boundary layer. Boundary-Layer Meteorol 83:75–98

Batchelor G (1949) Diffusion in a field of homogeneous turbulence. I. Eulerian analysis. Aust J Sci Res 2(437):437–450

Bélair S, Mailhot J, Strapp J, MacPherson J (1999) An examination of local versus nonlocal aspects of a TKE-based boundary layer scheme in clear convective conditions. J Appl Meteorol 38:1499–1518

Benoit R, Côté J, Mailhot J (1989) Inclusion of a TKE boundary layer parameterization in the Canadian regional finite-element model. Mon Wea Rev 117:1726–1750

Blackadar A (1962) The vertical distribution of wind and turbulent exchange in a neutral atmosphere. J Geophys Res 67:3095–3102

Bougeault P, Lacarrère P (1989) Parameterization of orography-induced turbulence in a mesobeta-scale model. Mon Wea Rev 117:1872–1890

Bradshaw P, Ferriss D, Atwell N (1967) Calculation of boundary-layer development using the turbulent energy equation. J Fluid Mech 28:593–616
Chen C, Cotton W (1983) Numerical experiments with a one-dimensional higher order turbulence model: simulation of the Wangara day 33 case. Boundary-Layer Meteorol 25:375–404
Cheng Y, Canuto V, Howard A (2002) An improved model for the turbulent PBL. J Atmos Sci 59:1550–1565
Cheng Y, Canuto V, Howard A (2005) Nonlocal convective PBL model based on new third- and fourth-order moments. J Atmos Sci 62:2189–2204
Clarke R, Dyer A, Brook R, Reid D, Troup A (1971) The Wangara experiment: boundary layer data. Technical Report 19, Commonwealth Scientific and Industrial Research Organization, 362 pp
Davies H (1983) The stability of some planetary boundary layer diffusion equations. Mon Wea Rev 111: 2140–2143
Davy R, Taylor P, Weng W, Li P (2009) A model of dust in the Martian lower atmosphere. J Geophys Res 114, 9 pp
Deardorff J (1974) Three-dimensional numerical study of the height and mean structure of a heated planetary boundary layer. Boundary-Layer Meteorol 7:81–106
Delage Y (1974) A numerical study of the nocturnal atmospheric boundary layer. Q J Roy Meteorol Soc 100:351–364
Delage Y (1997) Parameterising sub-grid scale vertical transport in atmospheric models under statically stable conditions. Boundary-Layer Meteorol 82:23–48
Deleersnijder E, Burchard H, Dijkstra H (2003) On the stability of turbulence closure schemes for stratified flows. NCTAM-2003-093, 5 pp
Detering H, Etling D (1985) Application of the $e - \epsilon$ turbulence model to the atmospheric boundary layer. Boundary-Layer Meteorol 33:113–133
Durbin P (1991) Near-wall turbulence closure modeling without damping functions. Theor Comput Fluid Dyn 3:1–13
Durbin P (1993) Application of a near-wall turbulence model to boundary layers and heat transfer. Int J Heat Fluid Flow 14:316–323
Duynkerke P, Driedonks A (1987) A model for the turbulent structure of the stratocumulus-topped atmospheric boundary layer. J Atmos Sci 44:43–64
Dyer A, Bradley E (1982) An alternative analysis of flux-gradient relationships at the 1976 ITCE. Boundary-Layer Meteorol 22:3–19
Galperin B, Kantha L, Hassid S, Rosati A (1988) A quasi-equilibrium turbulent energy model for geophysical flows. J Atmos Sci 45:55–62
Garratt J, Brost R (1981) Radiative cooling effects within and above the nocturnal boundary layer. J Atmos Sci 38:2730–2746
Girard C, Delage Y (1990) Stable schemes for nonlinear vertical diffusion in atmospheric circulation models. Mon Wea Rev 118:737–745
Gryning S, Batchvarova E, Brummer B, Jorgensen H, Larsen S (2007) On the extension of the wind prole over homogeneous terrain beyond the surface layer. Boundary-Layer Meteorol 124:251–268
Ha K-J, Mahrt L (2003) Radiative and turbulent fluxes in the nocturnal boundary layer. Tellus A 55:317–327
Hess G, Garratt J (2002) Evaluating models of the neutral, barotropic planetary boundary layer using integral measures: Part II. Modelling observed conditions. Boundary-Layer Meteorol 104:359–369
Hess G, Hicks B, Yamada T (1981) The impact of the Wangara experiment. Boundary-Layer Meteorol 20: 135–174
Holt T, Raman S (1988) A review and comparative evaluation of multilevel boundary layer parameterizations for first-order and turbulent kinetic energy closure schemes. Rev Geophys 26:761–780
Hunt J, Kaimal J, Gaynor J (1988) Eddy structure in the convective boundary layer—new measurements and new concepts. Q J Roy Meteorol Soc 114:827–858
Kaimal J, Finnigan J (1994) Atmospheric boundary layer flows. Oxford University Press, Oxford, 289 pp
Karcz M, Badur J (2005) An alternative two-equation turbulent heat diffusivity closure. Int J Heat Mass Transf 48:2013–2022
Launder B, Spalding D (1972) Lectures in mathematical models of turbulence. Technical Report, Department of Mechanical Engineering, Imperial College of Science and Technology, London, England, 169 pp
Launder B, Reece G, Rodi W (1975) Progress in the development of a Reynolds-stress turbulence closure. J Fluid Mech 68:537–566
Manins P (1982) The daytime planetary boundary layer: a new interpretation of Wangara data. Q J Roy Meteorol Soc 108:689–705
Noh Y, Cheon W, Hong S, Raasch S (2003) Improvement of the K-profile model for the planetary boundary layer based on large eddy simulation data. Boundary-Layer Meteorol 107:401–427

Patankar S (1980) Numerical heat transfer and fluid flow. Hemisphere Publications (McGraw-Hill Book Co.), New York. ISBN:0-07-0487404. 197 pp
Patankar S (1981) A calculation procedure for two-dimensional elliptic situations. Numer Heat Transf 4: 409–425
Pope S (2000) Turbulent flows. Cambridge University Press, Cambridge. ISBN: 0521591252. 806 pp
Rao K, Wyngaard J, Coté O (1974) Local advection of momentum, heat, and moisture in micrometeorology. Boundary-Layer Meteorol 7:331–348
Savijärvi H, Kauhanen J (2008) Surface and boundary-layer modelling for the Mars exploration rover sites. Q J Roy Meteorol Soc 134:635–641
Schaller E (1977) Time and height variability of the sensible heat flux in the surface layer. Boundary-Layer Meteorol 11:329–354
Siqueira M, Katul G (2010) A sensitivity analysis of the nocturnal boundary-layer properties to atmospheric emissivity formulations. Boundary-Layer Meteorol 134:223–242
Taylor G (1921) Diffusion by continuous movements. Proc Lond Math Soc 2 A20:196–211
Troen I, Mahrt L (1986) A simple model of the atmospheric boundary layer: sensitivity to surface evaporation. Boundary-Layer Meteorol 37:129–148
Weng W, Taylor P (2003) On modelling the one-dimensional atmospheric boundary layer. Boundary-Layer Meteorol 107:371–400
Witek M, Teixeira J, Matheou G (2011) An integrated TKE-based eddy diffusivity/mass flux boundary layer closure for the dry convective boundary layer. J Atmos Sci 68:1526–1540
Wyngaard J (2010) Turbulence in the atmosphere. Cambridge University Press, Cambridge, U.K. 393 pp
Wyngaard J, Coté O (1974) The evolution of a convective planetary boundary layer—a higher-order closure model study. Boundary-Layer Meteorol 7:289–308
Yamada T, Mellor G (1975) A simulation of the Wangara atmospheric boundary layer data. J Atmos Sci 32:2309–2329